SPE 89921

Impact of Relative Permeability Hysteresis on the Numerical Simulation of WAG Injection

Elizabeth J. Spiteri, SPE, Stanford U.; Ruben Juanes, SPE, Stanford U.

This paper was prepared for presentation at the SPE Annual Technical Conference and Exhibition held in Houston, Texas, U.S.A., 26–29 September 2004.

Abstract

Pore-scale physics, laboratory investigations, and field experience, dictate that three-phase relative permeabilities exhibit strong dependence on the saturation path and the saturation history. Such dependence is especially relevant in water-alternating-gas (WAG) processes, which are characterized by a sequence of three-phase drainage and imbibition cycles. In this paper, we study the influence of relative permeability hysteresis on the field-scale predictions of WAG injection.

Because their measurement is difficult and time-consuming, three-phase relative permeabilities are usually interpolated from two-phase data. The errors associated with this procedure have been investigated by Oak (SPE 20183), who reported that interpolated values may differ significantly from experimental ones. The effect of using different interpolation models in field-scale simulations has been illustrated by a number of authors, who found that recovery predictions could be significantly different depending on the three-phase relative permeability model.

Here, we study the impact of using *history-dependent* saturation functions in reservoir simulations. First, we investigate the degree of accuracy with which different hysteretic models reproduce Oak's three-phase relative permeability data. In doing so, we assess the validity of existing models, and we identify the model parameters subject to most uncertainty. Second, we illustrate how the use of a hysteretic relative permeability model affects reservoir simulations. We use a synthetic model of a quarter five-spot pattern in a homogenous reservoir, and a more realistic heterogeneous reservoir modified from the PUNQ-S3 model. We find that there is striking disparity in the simulation results depending on whether a hysteretic or a nonhysteretic model is employed, and conclude that it is essential to incorporate hysteresis in the relative permeabilities in order to obtain accurate predictions of realistic WAG processes.

Introduction

Quantitative predictions of multiphase flow in porous media are necessary for the evaluation and management of oil and gas reservoirs. In particular, the simultaneous flow of three separate phases (water, oil and gas) is essential in the characterization and modeling of a number of oil recovery processes, such as waterflooding in the presence of free gas, steam injection, and CO_2 flooding.[1] Three-phase flow conditions become especially relevant for recovery processes based on water alternating gas (WAG) injection.[2] Three-phase flows occur also in environmental applications such as geological CO_2 sequestration[3] and groundwater contamination by nonaqueous-phase liquids.[4]

These predictions are now performed routinely using numerical simulations tools. Even though reservoir models continue to increase in size and geometrical complexity, they still rely on a straightforward multiphase flow extension of Darcy's law.[5] The cornerstone of multiphase flow models is the relative permeability, which accounts for the reduction in flow due to the mutual interaction of the different flowing phases. Although traditionally understood as unique functions of saturation, there is conclusive theoretical and experimental evidence that relative permeabilities depend on many other rock and fluid descriptors, including rock wettability, fluid viscosity, interfacial tension, flow rate and, of special interest to us, saturation history.[6] However, because direct measurement of three-phase relative permeabilities is costly and very time consuming, it is standard practice to rely on two-phase relative permeability experimental data, and use and interpolation model to evaluate the relative permeabilities under three-phase flow conditions.

A large number of relative permeability models have been proposed (see, e.g. Ref. 7 for a historical overview). The most commonly-used interpolation models in reservoir simulators are Stone I,[8] Stone II,[9] and saturation-weighted interpolation.[10] However, it has been shown that the ability of most empirical or semi-empirical interpolation models to reproduce direct experimental measurements of three-phase relative permeabilities is quite limited.[10–15] The most severe limitation of simple interpolation models is their inability to reproduce hysteresis effects, that is, dependence on the saturation path and saturation history. Such dependence is the result of process-dependence in the microscopic contact angle, and

trapping of the nonwetting phase. A few relative permeability models have been developed that incorporate hysteresis effects.[16–22] Most of them have not yet been implemented in commercial reservoir simulators.

Several authors (e.g.[23,24]) have investigated the impact of using different *interpolation models* in numerical simulations, concluding that recovery predictions could be very different depending on the relative permeability model used. In this paper, we extend previous investigations by performing a quantitative analysis of three-phase relative permeability models that account for hysteresis effects. The objective of this paper is twofold: (1) assess the validity of hysteretic relative permeability models to reproduce experimental data; and (2) evaluate the impact of using different models in the simulation of oil recovery process, with emphasis on WAG injection. We should mention that an assessment of three-phase hysteretic relative permeability models by means of comparison with experimental data has recently been performed independently.[25]

An outline of the paper is as follows. In Section 2, we give a brief review of the relative permeability models typically implemented in reservoir simulators. We emphasize the importance of choosing appropriate two-phase relative permeability data, and revisit three-phase interpolation models and hysteresis models. In Section 3, we assess the performance of different relative permeability models by comparison with direct measurements of three-phase relative permeability for displacement scenarios representative of WAG injection. We use the experimental data from Oak,[13] which is one of the most comprehensive and reliable three-phase relative permeability data sets available. In Section 4, we illustrate the effect of the choice of the three-phase interpolation model and the hysteresis model on the reservoir simulation predictions. We report simulations on a very simple synthetic black-oil reservoir model, to isolate the impact of the relative permeability model. In Section 5, we extend the numerical investigation and perform simulations on a realistic three-dimensional heterogeneous reservoir, modified from the well-known PUNQ-S3 case study.[26,27] In the final section, we summarize the main conclusions of this investigation.

Review of relative permeability models

The Darcy flow formalism has theoretical justification for single-phase flow, but is simply an empirical approximation (sometimes rather crude) for multiphase flow. The relative permeabilities are the key parameters of Darcy-type models of multiphase flow, and they are left with the task of incorporating the complex physics of multiphase flow. They should be regarded as *functionals* of various fluid and rock descriptors, rather than unique functions of the fluid saturations.[28] However, measuring three-phase relative permeabilities for all displacement processes of interest is extremely costly and time consuming. As a result, many of the dependencies of relative permeabilities have been largely ignored in reservoir simulation, where it is common practice to understand three-phase relative permeabilities as unique functions of saturations, obtained from interpolation of two-phase data.

In this section, we review the most commonly used relative permeability models —specifically, oil interpolation models and gas hysteresis models— and assess the validity of these models by how accurately they reproduce experimental data.

Two-phase relative permeability data. The most common models estimate relative permeability of oil, water, and gas under three-phase conditions by interpolation of two-phase data. Independently of how this interpolation is carried out, it is essential that the two-phase experiments reproduce a similar saturation history to that of the three-phase scenario to be estimated. For example, if the reservoir undergoes primary production by internal gas drive followed by waterflooding, the appropriate two-phase experiments are: (1) a water-oil flow experiment, with increasing water saturation, and (2) a gas-oil flow experiment at connate water saturation, with increasing gas saturation. In a WAG process, three distinct displacements take place (**Fig. 1**): (1) imbibition from natural or man-made water drive, (2) gas flood into water and residual oil, and (3) waterflood into gas and residual oil. It is apparent that relative permeabilities along saturation path (3) —and subsequent gas and water injection— are less likely to be well represented by the two-phase experimental curves. In Section 3 we show that this is indeed the case.

From the two-phase input data, relative permeabilities are commonly estimated assuming: (1) water relative permeability is a function of water saturation only, (2) gas relative permeability is also a function of gas saturation only, and (3) oil relative permeability is a function of all three saturations.[13,29,30] In fact, this assumption is justified only if the rock is strongly water-wet, a condition that is rarely met in practice.

The *water relative permeability* is typically obtained from an oil-water imbibition or drainage experiment. For strongly water-wet rocks, the choice is not critical because the water relative permeabilities are almost the same. For simulation purposes, however, it is important that the water relative permeability be tabulated for the full range of water saturations from the connate water saturation S_{wc} to the maximum water saturation that can be achieved in the reservoir. For most enhanced oil recovery systems, the maximum water saturation is higher than that of the oil-water imbibition experiment, $1 - S_{or(w)}$, where $S_{or(w)}$ is the oil-to-water residual saturation. The water relative permeability from one of Oak's experiments is shown in **Fig. 2**.

The *gas relative permeability* would be measured in an oil-gas experiment at connate water saturation. As opposed to water, gas relative permeability is a strong function of saturation history. For the simulation of WAG systems, it is therefore necessary to consider a saturation path of decreasing gas saturation also. In **Fig. 3** we plot the gas relative permeability as a function of gas saturation for two such experiments.

Because *oil relative permeability* is regarded as dependent upon all saturations, one must enter two experimental curves: the imbibition water-oil experiment, $k^i_{ro(w)}$ (**Fig. 4**), and a drainage gas-oil experiment at connate water, $k^d_{ro(g)}$ (**Fig. 5**). Both experiments evolve in the direction of decreasing oil saturation.

Three-phase interpolation models. The water, gas, and oil relative permeabilities from the two-phase experiments described above are then used to determine oil relative permeabilities in three-phase systems. Because oil relative permeability is a function of all three fluid saturations, an interpolation model is used to predict the relative permeability in the three-phase region between the oil-water and gas-oil-connate water saturation paths. The most common interpolation models used in reservoir simulation are Stone I and Stone II. Another classic method is the saturation-weighted interpolation originally proposed by Baker.

The *Stone I* model is usually implemented in commercial simulators in the normalized version of Aziz and Settari[31]. The oil relative permeability obtained from the Stone I model is given by:

$$k_{ro} = \frac{S_o^* k^i_{ro(w)} k^d_{ro(g)}}{k_{ro(wc)}(1-S_w^*)(1-S_g^*)} \tag{1}$$

where

$$S_o^* = \frac{S_o - S_{or}}{1 - S_{wc} - S_{or}} \tag{2}$$

$$S_w^* = \frac{S_w - S_{wc}}{1 - S_{wc} - S_{or}} \tag{3}$$

$$S_g^* = \frac{S_g}{1 - S_{wc} - S_{or}} \tag{4}$$

are the normalized phase saturations. In Eq. (1), $k_{ro(wc)}$ is the oil relative permeability at connate water and critical gas saturations. We have assumed that the critical gas saturation is zero. It is important to note that $k^i_{ro(w)}$ is evaluated at $S_o = 1 - S_{wc}$, and $k^d_{ro(g)}$ is evaluated at $S_o = 1 - S_g - S_{wc}$, that is, at *different* oil saturations than the three-phase case being predicted. The residual oil saturation S_{or} is *not* a constant. It will take a different value depending on the amount of gas present, and should be considered as a (possibly nonlinear) function of gas saturation. If the residual oil saturation is known, it may be input as a function of gas or water saturation. When this information is not available, one can resort to one of the residual oil saturation models that have been proposed.[32] One possibility is to use a linear interpolation between the limiting values $S_{or(w)}$ and $S_{or(g)}$:

$$S_{or} = \alpha S_{or(w)} + (1-\alpha) S_{or(g)} \tag{5}$$

where

$$\alpha = 1 - \frac{S_g}{1 - S_{wc} - S_{or(g)}} \tag{6}$$

Often, the residual oil saturation is taken as the minimum of the residual oil of the same displacement processes:

$$S_{or} = \min(S_{or(w)}, S_{or(g)}) \tag{7}$$

In **Fig. 6** we plot the oil isoperms obtained using the Stone I interpolation model with the two-phase relative permeability data shown in **Figs. 2–5**. The isoperms are convex, especially in the region of low oil saturations.

The *Stone II model* does not require a separate interpolation of the residual oil saturation, and the model actually predicts this curve. In normalized form, the model is written as:

$$k_{ro} = k_{ro(cw)} \left[\left(\frac{k^{i}_{ro(w)}}{k_{ro(cw)}} + k^d_{rw(o)} \right) \left(\frac{k^{d}_{ro(g)}}{k_{ro(cw)}} + k^d_{rg(o)} \right) \right] \tag{8}$$

The two-phase relative permeabilities are evaluated at the same saturation values as in the Stone I model. In **Fig. 7** we plot the oil isoperms obtained with the Stone II model, when applied to the same two-phase relative permeability data. The relative permeability contours are convex near the OW edge, but become concave near connate water. The predicted values in the region of low oil saturation are much lower than those obtained with the Stone I method.

The saturation-weighted interpolation model (or *Baker model*) computes the oil relative permeability as:

$$k_{ro} = \frac{(S_w - S_{wc}) k^i_{ro(w)} + (S_g) k^d_{ro(g)}}{(S_w - S_{wc}) + S_g} \tag{9}$$

where the two-phase relative permeabilities are evaluated at the same oil saturation of the three-phase case, that is:

$$\begin{aligned} k^i_{ro(w)} &= k^i_{ro(w)}(1-S_o) = k^i_{ro(w)}(S_w + S_g) \\ k^d_{ro(g)} &= k^d_{ro(g)}(1-S_{wc}-S_o) = k^d_{ro(g)}(S_g + S_w - S_{wc}) \end{aligned} \tag{10}$$

The oil isoperms predicted by Baker are given in **Fig. 8**. Other more sophisticated saturation-weighted interpolation models exist,[20,21] but are not so widely used in reservoir simulation as the three discussed above.

Relative permeability hysteresis. Hysteresis refers to irreversibility, or path dependence. In multiphase flow, it manifests itself through the dependence of the relative permeabilities and capillary pressures on the saturation path and the saturation history. From the point of view of pore-scale processes, hysteresis has at least two sources: (1) contact angle hysteresis: the advancing contact angle (of wetting phase displacing a nonwetting phase) is much larger than the receding contact angle (of wetting phase retreating by nonwetting phase invasion); and (2) trapping of the nonwetting phase: during an imbibition process, a fraction of the nonwetting phase gets disconnected in the form of blobs or ganglia, becoming effectively immobile (trapped). Hysteresis effects are larger in processes with strong flow reversals. This is the case of WAG injection, in which the gas phase is trapped during waterflooding after a gas flood.

A number of hysteresis empirical models have been developed to characterize the relative permeabilities and trapped saturation of the non-wetting phase after a flow reversal. Experimental data strongly suggest that the nonwetting phase experiences much more pronounced hysteresis than the wetting phase. Therefore, in water-wet systems, the gas phase shows the largest hysteretic effects, and oil displays hysteresis in water-oil systems, but much less so in oil-gas displacements at connate water.

Two-phase hysteresis models. The most important quantity determining the significance of hysteresis effects is the trapped nonwetting-phase saturation after a flow reversal

(for trapped gas, we denote this saturation as S_{gt}). Most relative permeability models that incorporate hysteresis[16,18–21] are based on the trapping model proposed by Land.[33] In this model, the trapped nonwetting phase saturation is computed as:

$$S_{gt} = S_{gc} + \frac{S_{g,hy} - S_{gc}}{1 + C(S_{g,hy} - S_{gc})} \tag{11}$$

where S_{gc} is the critical gas saturation, $S_{g,hy}$ is the gas saturation at the flow reversal, and C is the Land trapping parameter. The Land coefficient is computed from the *bounding* drainage and imbibition curves as follows:

$$C = \frac{1}{S_{gt,\max} - S_{gc}} - \frac{1}{S_{g,\max} - S_{gc}} \tag{12}$$

where $S_{g,max}$ is the maximum gas saturation, and $S_{gt,max}$ is the maximum trapped gas saturation, associated with the imbibition bounding curve. All these quantities are illustrated in **Fig. 9**. The value of the Land trapping parameter is dependent on the type of rock and fluids.

Here, we describe two common models that incorporate hysteresis in two-phase systems: the model proposed by Killough[16] and the one proposed by Carlson.[17]

In *Killough's method*, the nonwetting phase relative permeability along a scanning curve —such as the one depicted in **Fig. 9**— is computed as:

$$k^i_{rg}(S_g) = \frac{k^i_{rg(o)}(S_{g,norm}) \cdot k^d_{rg(o)}(S_{g,hy})}{k^d_{rg(o)}(S_{g,\max})} \tag{13}$$

where

$$S_{g,norm} = S^i_{g(o)} + \frac{(S_g - S_{gt,\max})(S_{g,\max} - S^i_{g(o)})}{S_{g,hy} - S_{gt,\max}} \tag{14}$$

In Eq. (13), $k^i_{rg(o)}$ and $k^d_{rg(o)}$ represent the relative permeability values on the bounding imbibition and drainage curves, respectively.

In *Carlson's model*, the scanning curve is assumed to be parallel to the imbibition curve. It is obtained by shifting the bounding imbibition curve horizontally until it intersects the saturation at the flow reversal.

A common feature of both models (and most other "two-phase" relative permeability hysteresis models) is that the scanning *imbibition* curve is assumed to be representative of any subsequent *drainage* process. This "reversibility" of the relative permeability curves is exemplified in **Fig. 10** with an actual simulation using the Carlson model. As we demonstrate in the next section, this behavior is not supported by experimental data.

Three-phase hysteresis models. The assumption of reversibility of the drainage and imbibition scanning curves is inappropriate. Gas relative permeability is higher when displacing oil only than when displacing a water-oil mixture after a waterflood. As a result, relative permeabilities do not follow the secondary drainage path predicted by the two-phase models. In addition, it is often observed that water permeability is reduced after gas injection (although we have found that this is a second order effect). A number of so-called "three-phase" hysteresis models have been developed to account for irreversibility in the relative permeability scanning curves.[18,19,34,35]

The gas relative permeabilities on the scanning curves are modeled by:

$$k^i_{rg}(S_g) = k^d_{rg(o)}(S_{gf}) \tag{15}$$

where S_{gf} is a flowing gas saturation,

$$S_{gf} = S^d_{g(o)} + \frac{1}{2}\left\{(S_g - S_{gt,\max}) + \sqrt{(S_g - S_{gt,\max})^2 + \frac{4}{C}(S_g - S_{gt,\max})}\right\} \tag{16}$$

and the drainage relative permeability curve is given by:

$$k^d_{rg} = \left[k^d_{rg(o)} - k^d_{rg(o)}\left(S_g^{start}\right)\right] \cdot \left[\frac{S_{wc}}{S_w^{start}}\right]^{\alpha} + \left[k^d_{rg(o)}\left(S_g^{start}\right)\right] \tag{17}$$

Therefore, the required data is the drainage bounding relative permeability curve $k^d_{rg(o)}(S_g)$, the Land trapping coefficient C, and a secondary drainage reduction coefficient α. A representative evolution of the gas relative permeability after a sequence of water and gas floods is shown in **Fig. 11**. The model accounts for cyclic irreversibility, and the differences with respect to **Fig. 10** are apparent.

Comparison with relative permeability data

We investigate the accuracy of relative permeability models by comparing the model predictions with experimental data. We used the experimental data of Oak,[13] which is one of the most extensive and reliable data sets available. It comprises over 2000 two-phase and three-phase relative permeability measurements, following a wide range of saturation paths. We selected the experiments corresponding to the saturation paths shown in **Fig. 12**. The individual experiments can be organized into three experiments (Experiments 1–3), each of which consists in a sequence of four different saturation paths. *Path 1* corresponds to a water-oil drainage experiment where oil is injected until connate water saturation is reached. *Path 2* is a water-oil imbibition experiment, which continues until residual oil. *Path 3* simulates a gas injection process, in which oil is expelled from the system, reaching a lower residual value. *Path 4* is representative of waterflooding after a gas flood; water is injected, displacing gas and some additional oil which had previously been remobilized during the gas injection phase.

Several measurements of relative permeability were taken along each displacement path. For each saturation state, we compare relative permeabilities calculated from different models with the actual relative permeabilities measured in the experiment. We illustrate graphically the accuracy of the model by constructing a scatter plot of calculated vs. measured relative permeability. We investigate separately the validity of the water permeability model, the oil interpolation model, and the gas hysteresis model.

Water relative permeabilities. Our objective here is to evaluate the common assumption that water relative permeability is a function of water saturation alone, and independent of the saturation history. We compare the water

relative permeability measured along each of the displacement paths 1–4 against the "modeled" water relative permeability —which is nothing else than the curve in **Fig. 2**, corresponding to a drainage oil-water displacement. We construct the scatter plots in **Fig. 13** by gathering the water saturations from each experiment, interpolating their water relative permeabilities from the drainage curve in **Fig. 2**, and plotting them against the experimental values. The predicted relative permeabilities for the first displacement path are accurate for all three experiments. In the following imbibition process (path 2), the predicted relative permeabilities slightly underestimate the measured values at low saturations. During the gas injection process (path 3), the water relative permeabilities marginally overestimate the experimental values. The largest errors in the predictions occur for path 4, that is, a waterflood after a gas flood. The predicted relative permeabilities overestimate the experimental values. This is consistent with the observation that water mobility is reduced after a gas flood.[36] We conclude, however, that for most displacement processes in water-wet media, water relative permeabilities obtained from a drainage experiment are sufficiently accurate.

Three-phase interpolation models for oil relative permeability. We investigate the accuracy of Stone I, Stone II, and Baker models for interpolating oil relative permeability from two-phase data. As a preliminary step, we analyze the variability of measured oil relative permeabilities along the two-phase paths (paths 1 and 2). The scatter plots in **Fig. 14** were obtained by comparing the interpolated data from **Fig. 4** with the measured oil relative permeability from each experiment. The variability is small for the drainage experiment. For the imbibition experiment, however, the predicted relative permeabilities are accurate for high oil saturations but show more variability for low oil saturations.

We now assess the validity of interpolation models for oil relative permeability in three-phase flow scenarios (paths 3 and 4). Interpolated values are plotted against measured relative permeabilities to generate scatter plots.

The correlation between experimental and predicted oil relative permeability using the *Stone I* method is shown in **Fig. 15**. Eq. (7) was used to model the residual oil saturation. Other residual oil models produced a less satisfactory correlation. In a gas injection process (path 3), the Stone I model predicts the oil relative permeability well for high oil saturations, but overestimates oil relative permeabilities as saturations decrease. For a waterflood after gas injection (path 4), Stone I yields a fair prediction in this case.

The oil relative permeability correlation obtained with the *Baker model* is shown in **Fig. 16**. For path 3, the correlation is good in the region of low oil saturations, but the model significantly underestimates the relative permeability for oil saturations greater than 0.01. For path 4, the Baker model underestimates the oil relative permeability for the entire saturation span.

The *Stone II model* underestimates the relative permeabilities for paths 3 and 4 so severely, that the scatter plot does not give any information. This result was expected, given that the saturation paths are in the region where Stone II predicts zero permeability (**Fig. 17)**.

In conclusion, when compared to experimental data, the Stone I model performed the best relative to Stone II and Baker for both processes of interest (gas injection and water injection) and for low and high oil saturations. The residual oil saturation model given by Eq. (7) gave a better correlation than linear interpolation.

Gas phase relative permeabilities. In this section we investigate the validity of relative permeability models for the gas phase. We test first if the gas relative permeability can be understood as a nonhysteretic function of gas saturation alone by comparing the gas relative permeability from the experimental data for paths 3 and 4, with the interpolated gas relative permeability from the input two-phase data (**Fig. 3)**. The corresponding scatter plot is shown in **Fig. 18**. During the gas injection process (path 3), the predicted relative permeabilities are slightly higher than the experimental ones, and the disparity is larger in the region of low gas saturations. However, during the imbibition process of water injection after a gas flood (path 4), the two-phase relative permeabilities overestimate the three-phase experimental, because trapping of gas is unaccounted for. It is therefore imperative that the reduction in gas relative permeability is incorporated with appropriate hysteresis models. The validity of these models is addressed in next.

Land trapping coefficient. Since most nonwetting phase hysteresis models are based on the trapping model proposed by Land,[33] we investigate the validity of such model with the data available. A rigorous analysis of its validity would require a series of scanning curves with different gas saturations $S_{g,hy}$ at flow reversal. One would then compare the predicted trapped gas saturation S_{gt} obtained from Eq. (11) with the experimental one. We did not have access to this type of experimental data, and we limited our analysis to computing the Land trapping coefficient from the bounding drainage and imbibition curves of Oak's two-phase experiments. Values of the Land trapping coefficient for different experiments are plotted (in increasing order) in **Fig. 19**. The experiments are grouped by the pair of fluids (water-gas, oil-gas, or water-oil), and the rock sample (200 md, 800 md, or 1000 md Berea sandstone). It is apparent that the Land parameter is far from being constant. We recall that, according to Eq. (11), large values of C indicate *less* nonwetting phase trapping. The value of the Land trapping parameter depends crucially on the pair of fluids used, and the permeability of the medium. For the same permeability, C decreases —and therefore trapping increases— as the interfacial tension between the fluids increases. For example, the Land parameter for a water-gas system is lower than for a water-oil system. For the same pair of fluids, C decreases as the permeability of the sample decreases. Both trends are consistent with the observation that trapping of the nonwetting phase increases as capillary effects become dominant. In the case of Oak's experiments, the Land coefficient varies between 0.7 and 2.2. Such variation illustrates the need for a judicious choice of the Land trapping parameter in numerical simulations. In addition, a recent study[25] has shown that, for an intermediate-wet rock, the Land trapping coefficient will also vary between hysteresis cycles. They found that the Land

parameter increases for each subsequent waterflood, indicating that the trapped gas saturation decreases.

Two-phase hysteresis models. We now test the applicability of two-phase hysteresis models of gas relative permeability to a three-phase imbibition process. The use of these models imply the assumption of reversibility of the imbibition scanning curves during a subsequent drainage process (**Fig. 10)**. This behavior is not supported by experimental data. In **Fig. 20** we plot the oil relative permeability measured in an oil-water experiment —where oil is the nonwetting phase— which shows clearly that the imbibition scanning curve is *not* reversible.

In **Fig. 21** we show the comparison between the gas relative permeability predicted by Killough's two-phase hysteresis method and experimental data corresponding to water injection after a gas flood (path 4). As anticipated from **Fig. 20**, the model overestimates gas relative permeability significantly. The gas relative permeability correlation for path 4 using Carlson's method is shown in **Fig. 22**. Because this method uses the entire bounding imbibition curve (instead of the Land trapping parameter alone), the agreement between model and experiments is better. However, the gas relative permeabilities are consistently overestimated as well.

Three-phase hysteresis models. These models relax the assumption of reversibility of scanning curves, and allow for reduction of the gas relative permeability during gas injection following a waterflood. The method by Larsen and Skauge[34] uses the Land trapping coefficient C and the permeability reduction parameter α to define the scanning curves. The correlation between predicted and experimental gas relative permeabilities along path 4 is shown in **Fig. 23**. Predictions improve —albeit slightly— with respect to Killough's model on which the three-phase model is based. It is possible, however, that the agreement could improve with an optimal choice of the reduction coefficient α.

Summary and discussion. We summarize the main findings from our analysis of Oak's experimental data in the following four points:

(1) In water-wet rocks, the water relative permeability does not show significant dependence on the saturation path or saturation history. Experimental data show, however, a slight reduction in water mobility after a gas flood.
(2) Commonly used interpolation models of oil relative permeability yield very different results, especially in the region of low oil saturation. The residual oil saturation model to be used in combination with Stone I interpolation should be carefully chosen (in our case, the model given in Eq. (7) performed better than linear interpolation). The Stone II method may severely underestimate the oil relative permeability.
(3) The Land trapping coefficient is a crucial parameter in many hysteretic relative permeability models. Experimental data suggest that this coefficient may vary significantly depending on the interfacial tension between the fluids and the permeability of the medium.
(4) Hysteretic relative permeability models currently available in commercial reservoir simulators,[16,17,34] tend to overestimate the gas relative permeability during cyclic water/gas injection.

The limited ability of commonly used relative permeability models to reproduce water-alternating-gas three-phase scenarios translates into a source of uncertainty in the numerical simulations. In the following two sections, we illustrate the impact that the choice of the relative permeability model has on *field-scale predictions*, which can impact the selection of recovery strategies and other reservoir management decisions.

Representative numerical simulations

In this section we report the results of numerical simulations for a synthetic, homogeneous, two-dimensional reservoir. The complexity of the reservoir model was kept to a minimum, in order to isolate the effects of (1) the oil relative permeability interpolation model, and (2) the hysteretic model. We used the commercial black-oil simulator Eclipse 100.[36]

Description of the model. We consider a quarter of a five-spot pattern in a homogeneous, horizontal reservoir (**Fig. 24**). The porosity is 0.2 and the horizontal permeability is 200 md, which coincides with the absolute permeability of the core from which the relative permeability values were measured. The domain is discretized into 25×25×1 grid blocks, each of dimension 40×40×100 ft. The total pore volume is 2×10^7 ft^3.

We used relative permeability data from the Oak experiments, reported in **Figs. 2–5**. Capillary pressure was ignored in this study. We employed very simple PVT data, representative of immiscible fluids (dead oil and dry gas). For simplicity, we took the water density and viscosity as 62.4 lb/ft^3 and 1 cp, respectively. The oil density and viscosity are 43.7 lb/ft^3 and 2 cp, respectively. The formation volume factor of water and oil is taken as exactly 1 rb/stb. The PVT properties of gas are given in **Table I** as functions of pressure. The gas density at a reference pressure of 14.7 psia is 0.063 lb/ft^3. At average reservoir conditions (about 2000 psia), the gas formation volume factor is approximately equal to 1 rb/stb, and the gas viscosity is approximately equal to 0.02 cp.

The reservoir is initially saturated with oil and connate water, and the initial reservoir pressure is 2000 psia. During the first five years, one pore volume of water is injected. After water injection, most of the reservoir contains oil at residual saturation to water. Since the residual oil saturation to gas is significantly lower than the residual oil saturation to water ($S_{org} < S_{orw}$), gas is then injected to produce more oil. A WAG injection scheme is then adopted, by injecting and producing one pore volume of fluid every five years, with a 1:1 WAG ratio. The injectors are controlled by voidage replacement, so the volume of fluid injected is the same as the volume produced. The producer is set to a target oil rate of 1000 rb/day, with a limit in the bottom hole pressure (BHP) of 1900 psi.

The effect of the interpolation model and the hysteresis model was studied by comparing recovery efficiencies, saturation paths, gas-oil ratios (GOR), and watercut (WCT).

Effect of the three-phase interpolation model. Recovery efficiency —the ratio of cumulative oil production to original oil in place— predicted by different interpolation models is shown in **Fig. 25**. The recovery efficiency after 30 years of production varies between 50.8% and 57.9% (a 14.0% difference) depending on the interpolation model used. The Stone I model predicts the highest recovery and the saturation-weighted model (Baker) predicts the lowest. This result can be easily explained in terms of the oil isoperms calculated by each model. In **Figs. 26–28** we plot the oil isoperms predicted by Stone I, Stone II and Baker, respectively, as well as the path describing the evolution of the fluid saturations in a grid block at the center of the reservoir model. The initial saturation state is marked with a square (□), and corresponds to a porous medium saturated with oil and connate water. During the first waterflood, the oil saturation decreases and the water saturation increases. Since the reservoir is under two-phase conditions, the saturation path corresponding to the initial waterflood is identical for all three interpolation models. Differences arise, however, during gas injection. Because of the convexity of the oil isoperms in the Stone I model, the oil relative permeability increases significantly, from a value of 0.001 at the end of the water flood to 0.05 at the end of gas injection. An analogous increase occurs for the Stone II model. For the Baker model, on the other hand, the oil isoperm is essentially parallel to the saturation path, and the oil relative permeability is less than 0.01 throughout the gas injection process. This marked difference in the shape of the oil isoperms explains the much lower recovery predicted by the Baker model. We recall that the Stone I model is the one that agrees with experimental data best.

Effect of the hysteresis model. We study the impact of relative permeability hysteresis on WAG simulation. We included in our analysis the hysteretic models of Killough and Carlson, as well as the three-phase extension due to Larsen and Skauge. We used the same two-phase relative permeability data as described before. Whenever necessary, we employed the Land trapping coefficient $C = 0.78$ —obtained from the two-phase relative permeabilities— and a reduction coefficient $\alpha = 0.01$.

We analyzed all possible combinations of hysteresis models for the gas phase —Killough, Carlson and WAG— and interpolation models for the oil phase —Stone I, Stone II and Baker. A summary of the results for all the test cases is given in **Table II**. As an illustrative example, we plot in **Fig. 29** the recovery efficiency predicted for different hysteresis models, when the Stone I interpolation model is used. The base case corresponds to the simulation with no hysteresis which, as described earlier, attains a recovery efficiency of 57.9% after 35 years of production. During the initial WAG cycle —the first ten years— all models give the same results because the system has not experienced a flow reversal yet. Differences arise between the hysteretic and nonhysteretic models at the beginning of the second WAG cycle, because gas is trapped during water injection. The two-phase and three-phase models, however, give essentially the same predictions. This is no longer the case after the second gas injection phase, because the three-phase model accounts for the reduction in the gas relative permeability, whereas the two-phase models do not. Reduced gas mobility results in a better sweep efficiency, therefore explaining the improved recovery predicted by the three-phase model.

Effect of the Land trapping coefficient. Most hysteresis models need a Land trapping coefficient as input, which is used to characterize the amount of trapped gas saturation at the flow reversal. The Land parameter depends on fluid and rock properties, and the displacement process. From the analysis of Oak's experimental data, we saw that the value Land trapping coefficient takes values between 0.5 and 2.0. Here, we analyze the sensitivity of WAG simulations to the Land trapping coefficient. We run simulations using the Stone I interpolation model and the three-phase WAG hysteresis model, with different values of C. In **Fig. 30** we plot the recovery efficiency obtained for different values of the Land trapping coefficient. The simulated recovery increases as the trapping coefficient decreases. A smaller trapping coefficient indicates higher trapped gas saturation during an imbibition process and, as a result, better sweep efficiency and higher simulated recovery. The improvement in recovery efficiency from the base case —no hysteresis— is 9% and 16%, for a Land trapping coefficient of 2.0 and 0.5, respectively.

Summary and discussion. Hysteresis effects are in fact responsible for the efficacy of water-alternating-gas injection. Water injection after a gas flood traps some of the free gas present in the reservoir. This is shown in **Fig. 31**, where we plot the evolution of saturations at a location of the reservoir during a WAG process, as predicted by hysteretic and nonhysteretic relative permeability models. Hysteretic models account for the fact that not all gas is displaced after water injection. Trapping of the gas phase is indeed beneficial, as it reduces the overall gas mobility, which results in better sweep efficiency and fluid production with lower gas-oil ratio (GOR), as shown in **Fig. 32**.

The results of the simulations presented here indicate that WAG simulation is quite sensitive to the treatment of relative permeability hysteresis. Depending on the hysteretic model used, predictions of oil recovery may be as much as 15% higher than without hysteresis (**Table II**). Among the different models typically available in reservoir simulators, the largest improvements in recovery predictions are obtained with the three-phase WAG hysteresis model in combination with the Stone I interpolation method. This choice is precisely the one that agrees with experimental data best.

WAG injection in a realistic reservoir

We now extend our study of the impact of relative permeability hysteresis on WAG injection to a realistic reservoir. The objective is to determine whether hysteresis continues to play an important role for geometrically complex, heterogeneous reservoir models with multiple injection and production wells. For this purpose we selected the PUNQ-S3 model, which is a well-known reservoir model originally developed as a test case for production forecasting under uncertainty. All the simulations were conducted with the Eclipse 100 black-oil reservoir simulator.

Description of the model. The original PUNQ-S3 model is described in detail elsewhere,[26] and the model data is publicly available for download.[27] We modified the original model slightly to study hysteresis effects by implementing a WAG injection scenario.

The geometry of the model is characterized by a dome with a small gas cap in the center. It is bounded by sealing faults on all sides and contains five layers of fluvial sand and shale. The top of the reservoir is at a depth of 7677 ft. The average reservoir thickness is 92 ft. The reservoir is discretized into 19×28×5 grid blocks, of which 1761 blocks are active. The *x* and *y* dimension of each block is 590 ft. The average porosity is 0.2, and the average horizontal permeability is 100 md. The anisotropy ratio is about 3. A map of the absolute permeability is shown in **Fig. 33**. The reservoir pore volume is almost 200 million barrels with an initial oil saturation of about 60% and an initial reservoir pressure of 3670 psia. The fluid distribution map is shown in **Fig. 34**.

We modified the original PUNQ-S3 model by changing the injection and production scheme, and the fluid composition. We used the same PVT and relative permeability data as in the synthetic model of the previous section. Well locations are also slightly different from the original model. Our model has four injection wells and four production wells, open to the third, fourth, and fifth layers of the reservoir. The production wells operate at a fixed bottom hole pressure of 2000 psia. The injection wells are rate controlled, and inject 6290 rb/day each (25,160 rb/day total). The WAG ratio is 1:1 with a slug size of 0.1 pore volumes, which was found to be an optimum operation scheme.[37] We simulated three WAG cycles of 2500 days each for a total simulation time over 7500 days (21 years).

Here we test the sensitivity of the interpolation model and the hysteresis models against a base case model without hysteresis.

Effect of the interpolation model. The oil recovery efficiency for different interpolation models (Stone I, Stone II and Baker) is plotted in **Fig. 35**. As for the synthetic case, the Stone I model predicts the highest recovery. In this case, the Stone II and Baker models give very similar results. The models deviate from one another during the gas injection phases, which is when a large fraction of the reservoir is in three-phase flow conditions. The difference in predicted recovery between the Stone I and Baker models after 25 years of production is about 7.9%, which is less than the differences observed in the synthetic case. Here, the impact of the interpolation model is slightly less significant because of the effects of gravity and heterogeneity.

Effect of the hysteresis model. The impact of using a hysteretic relative permeability model for oil recovery prediction is shown in **Fig. 36**. Recovery efficiency obtained by using Killough's two-phase hysteresis model and the WAG three-phase hysteresis model, is compared with the recovery efficiency predicted with a nonhysteretic model. Differences of up to 9.4% in ultimate recovery are obtained. Although not as dramatic as for the synthetic case, the impact of relative permeability hysteresis is still very significant. For this system, the choice of incorporating hysteresis effects is more important than the interpolation model used for the oil relative permeability. A summary of the results from the simulations of the PUNQ-S3 model is given in **Table III**.

Conclusions

The results of this investigation support the view that WAG injection cannot be modeled correctly without accounting for hysteresis effects. Our analysis has two key components: (1) evaluating the ability of several widely used three-phase relative permeability models to reproduce experimental data under WAG conditions, and (2) assessing the impact of the choice of the interpolation model and the hysteresis model on the simulation of WAG processes.

We used the three-phase relative permeability data of Oak[13] for the validation of relative permeability models. We found that the most common relative permeability interpolation models[8–10] yield very different results, especially in the region of low oil saturation. This is precisely the region of interest in WAG applications. Common "two-phase" hysteretic models[16,17] account for trapping of the nonwetting phase, but fail to reproduce the irreversibility of relative permeability scanning curves. When implemented in reservoir simulators, these models overestimate the gas relative permeability during gas injection following a waterflood. Extensions of these models to account for the lower gas permeability in secondary drainage processes[34] seem to be insufficient to capture the full extent of the gas mobility reduction. Most hysteretic relative permeability models are based on the theory proposed by Land.[33] The key parameter of the formulation is the trapping coefficient, which describes the trapped nonwetting phase saturation after a flow reversal. In this paper we show conclusive evidence that the Land trapping coefficient decreases —that is, the trapped nonwetting phase saturation increases— with increasing interfacial tension between the fluids, and decreasing permeability of the medium.

We then investigated the impact of the relative permeability model on the numerical prediction of field-scale WAG processes. We first analyzed a simple two-dimensional, homogeneous reservoir, to isolate the effects of the oil interpolation model and the gas hysteresis model. We found that "three-phase" hysteresis models lead to much larger recovery predictions than nonhysteretic models, because they account for the reduced mobility due to trapping of the gas phase during water injection. Depending on the interpolation model used, the difference in recovery efficiency could be as large as 15%. These findings were then confirmed by the simulation of WAG injection in the PUNQ-S3 model: a realistic, three-dimensional, heterogeneous reservoir, with multiple injection and production wells.

Acknowledgements

We gratefully acknowledge financial support from all members of the Stanford University Petroleum Research Institute for Gas Injection (SUPRI-C).

Nomenclature

k_{rw} = water relative permeability in a three-phase displacement
$k_{rw(o)}$ = water relative permeability in a water-oil displacement
k_{ro} = oil relative permeability in a three-phase displacement
$k_{ro(w)}$ = oil relative permeability in a water-oil displacement
$k_{ro(g)}$ = oil relative permeability in an oil-gas displacement
$k_{ro(wc)}$ = oil relative permeability at connate water displacement
k_{rg} = gas relative permeability in a three-phase displacement
$k_{rg(o)}$ = gas relative permeability in an oil-gas displacement
S_w = water saturation
S_o = oil saturation
S_g = gas saturation
$S_{g(o)}$ = gas saturation in an oil-gas displacement
S_{wc} = connate water saturation
$S_{or(w)}$ = residual oil saturation to water
$S_{or(g)}$ = residual oil saturation to gas
S_{or} = residual oil saturation in a three-phase displacement
S_{gc} = critical gas saturation
S_{gt} = trapped gas saturation
S_{gf} = flowing gas saturation
α = secondary drainage reduction exponent
C = Land trapping coefficient
$S_{gt,\max}$ = maximum trapped gas saturation
$S_{g,hy}$ = gas saturation at the flow reversal

References

1. Lake, L.W.: *Enhanced Oil Recovery*, Prentice Hall, upper Saddle River, New Jersey (1989).
2. Christensen, J.R., Stenby, E.H., Skauge, A.: "Review of WAG Field Experience," *SPEREE* (April 2001) 97–106.
3. Koide, H., Tazaki, Y., Noguchi, Y., Nakayama, S., Iijima, M., Ito, K., and Shindo, Y.: "Subterranean Containment and Long-Term Storage of Carbon Dioxide in Unused Aquifers and in Depleted Natural Gas Reservoirs," *Energy Conv. Manag.* (1992) **33**(5–8), 619–626.
4. Abriola, L.M., and Pinder, G.F.: "A Multiphase Approach to the Modeling of Porous Media Contamination by Organic Compounds, 1. Equation Development," *Water Resour. Res.* (1985) **21**(1), 11–18.
5. Muskat, M.: *Physical Principles of Oil Production*, McGraw-Hill, New York (1949).
6. Avraam, D.G., and Payatakes, A.C.: "Flow Regimes and Relative Permeabilities During Steady-State 2-Phase Flow in Porous Media," *J. Fluid Mech.* (1995) **293**, 207–236.
7. Juanes, R.: *Displacement Theory and Multiscale Numerical Modeling of Three-Phase Flow in Porous Media*, PhD Dissertation, U. of California at Berkeley (2003).
8. Stone, H.L.: "Probability Model for Estimating Three-Phase Relative Permeability," *JPT* (February 1970) 214–218; *Trans.*, AIME, **249**.
9. Stone, H.L.: "Estimation of Three-Phase Relative Permeability and Residual Oil Data," *J. Can. Petrol. Technol.* (1973) **12**(4), 53–61.
10. Baker, L.E: "Three-Phase Relative Permeability Correlations," paper SPE/DOE 17369 presented at the SPE/DOE Enhanced Oil Recovery Symposium, Tulsa, Oklahoma, April 17–20, 1988.
11. Delshad, M., and Pope, G.A: "Comparison of Three-Phase Oil Relative Permeability Models," *Transp. Porous Media* (1989) **4**, 59–83.
12. Oak, M.J., Baker, L.E., and Thomas, D.C.: "Three-Phase Relative Permeability of Berea Sandstone," *JPT* (August 1990) 1054–1061; *Trans.*, AIME, **289**.
13. Oak, M.J.: "Three-Phase Relative Permeability of Water-Wet Berea," paper SPE/DOE 20183 presented at the SPE/DOE Symposium on Enhance Oil Recovery, Tulsa, Oklahoma, April 22–25, 1990.
14. Hicks Jr., P.J., and Grader, A.S.: "Simulation of Three-Phase Displacement Experiments," *Transp. Porous Media* (1996) **24**, 221–245.
15. Oliveira, L.I., and Demond, A.H.: "Estimation of Primary Drainage Three-Phase Relative Permeability for Organic Liquid Transport in the Vadose Zone," *J. Contam. Hydrol.* (2003) **66**, 261–285.
16. Killough, J.E.: "Reservoir Simulation with History-Dependent Saturation Functions," *SPEJ* (February 1976) 37–48; *Trans.*, AIME, **261**.
17. Carlson, F.M.: "Simulation of Relative Permeability Hysteresis to the Nonwetting Phase," paper SPE 10157 presented at the SPE Annual Technical Conference and Exhibition, San Antonio, Texas, 1981.
18. Lenhard, R.J., Parker, J.C.: "A Model for Hysteretic Constitutive Relations Governing Multiphase Flow, 2. Permeability-Saturation Relations," *Water Resour. Res.* (1987) **23**(12), 2197–2206.
19. Lenhard, R.J., Oostrom, M.: "A Parametric Model for Predicting Relative Permeability–Saturation–Capillary Pressure Relationships of Oil-Water Systems in Porous Media With Mixed Wettability," *Transp. Porous Media* (1998) **31**, 109–131.
20. Jerauld, G.R.: "General Three-Phase Relative Permeability Model for Prudhoe Bay," *SPERE* (November 1997) 255–263.
21. Blunt, M.J.: "An Empirical Model for Three-Phase Relative Permeability," *SPEJ* (December 2000) 435–445.
22. Kjosavik A., Ringen J.K., and Skjaeveland S.M.: "Relative Permeability Correlation for Mixed-Wet Reservoirs," *SPEJ* (March 2002) 49–58.
23. Sato, K., and Aziz, K.: "Sensitivity of Steam Displacement Predictions to Three-Phase Relative Permeability Models," paper SPE 16733 presented at the SPE Annual Technical Conference and Exhibition, Dallas, Texas, September 27–30, 1987.
24. Guzman, R.E., Giordano D., Fayers F.J., Aziz K., Godi A.: "Three-Phase Flow in Field-Scale Simulation of Gas and WAG Injections," paper SPE 28897 presented at the European Petroleum Conference, London, U.K., October 25–27, 1994.
25. Element, D.J., Masters, J.H.K, Sargent, N.C., and Jayasekera A.J.: "Assessment of Three-Phase Relative Permeability Models Using Laboratory Hysteresis Data," paper SPE 84903 presented at the SPE International Improved Oil Recovery Conference, Kuala Lumpur, Malaysia, October 20–21, 2003.
26. Floris, F.J.T., Bush, M.D., Cuypers, M., Roggero, F., and Syversveen, A.R.: "Methods for Quantifying the Uncertainty of Production Forecasts: a Comparative Study," *Petrol. Geosci.* (2001) **7**(Sp.Iss.), S87–S96.

27. "PUNQ Case Studies," Netherlands Institute of Applied Geoscience, http://www.nitg.tno.nl/punq/cases/index.shtml
28. Juanes, R., and Patzek, T.W.: "Three-Phase Displacement Theory: An Improved Description of Relative Permeabilities", paper SPE 77539 presented at the SPE Annual Technical Conference and Exhibition, San Antonio, Texas, September 29–October 2, 2002, to appear in *SPEJ*.
29. Leverett, M.C., and Lewis, W.B.: "Steady Flow of Gas-Oil-Water Mixtures Through Unconsolidated Sands," *Trans.*, AIME (1941) **142**, 107–116.
30. Corey, A., Rathjens, C., Henderson, J., and Wyllie, M.: "Three-Phase Relative Permeability", *Trans.*, AIME (1956) **207**, 349–351.
31. Aziz, K., and Settari, A.: *Petroleum Reservoir Simulation*, Elsevier, London (1979).
32. Fayers, F.J., and Matthews, J.D.: "Evaluation of Normalized Stone's Methods for Estimating Three-Phase Relative Permeabilities," *SPEJ* (April 1984), 224–232; *Trans.*, AIME, **277**.
33. Land, C.S.: "Calculation of Imbibition Relative Permeability for Two- and Three-Phase Flow From Rock Properties." *SPEJ* (June 1968) 149–156; Trans., AIME, **243**.
34. Larsen, J.A., and Skauge, A.: "Methodology for Numerical Simulation with Cycle-Dependent Relative Permeabilities," *SPEJ* (June 1998), 163–173.
35. Egermann, P., Vizika, O., Kallet, L., Requin, C., Sonier, F.: "Hysteresis in Three-Phase Flow: Experiments, Modelling and Reservoir Simulations," paper presented at the IEA Workshop and Symposium on Enhanced Oil Recovery, Edinburgh, Scotland, September 20–22, 2000.
36. "ECLIPSE 100 Technical Description," Schlumberger GeoQuest, 2003.
37. Cakici, M.D.: "Cooptimization of Oil Recovery and Carbon Dioxide Storage," MS Thesis, Stanford U. (2003).

SI Metric Conversion Factors

bbl	× 1.589 873	E-01	=	m^3
cp	× 1.0*	E-03	=	Pa.s
ft	× 3.048*	E-01	=	m
ft^3	× 2.831 685	E-02	=	m^3
lbm/ft^3	× 1.601 850	E-02	=	g/cm^3
md	× 9.869 233	E-04	=	mm^2
psi	× 6.894 757	E+00	=	kPa
°F	(°F-32)/1.8		=	°C

* Conversion is exact.

Table I- Dry gas PVT properties

Pressure (psia)	Gas FVF (rb/stb)	Viscosity (cp)
14.7	192.5	0.0107
145	18.99	0.0109
290.1	9.242	0.0111
435.1	5.997	0.0114
580.2	4.374	0.0117
725.2	3.404	0.0121
870.2	2.759	0.0126
1015.3	2.301	0.0131
1305.3	1.699	0.0144
1740.5	1.199	0.0171
2175.6	0.928	0.0205

Table II- Summary of simulation results for the synthetic reservoir test case.

Case	Recovery Scheme	Hysteresis Model	Interpolation Model	Land Parameter (C)	% Recovery	% Difference from base case
1	**Waterflood (Base Case 1)**	None	None	N/A	49.0%	0.0%
2	**WAG (Base Case 2)**	None	Baker	N/A	50.8%	0.0%
3	**WAG (Base Case 2)**	None	Stone I	N/A	57.9%	0.0%
4	**WAG (Base Case 2)**	None	Stone II	N/A	55.9%	0.0%
5	WAG	Carlson	Baker	0.78	53.2%	4.7%
6	WAG	Carlson	Stone I	0.78	63.4%	9.5%
7	WAG	Carlson	Stone II	0.78	60.1%	7.5%
8	WAG	Killough	Baker	0.78	53.3%	4.9%
9	WAG	Killough	Stone I	0.78	62.8%	8.5%
10	WAG	Killough	Stone II	0.78	60.0%	7.3%
11	WAG	3 Phase WAG	Baker	0.78	53.5%	5.3%
12	WAG	3 Phase WAG	Stone I	0.78	66.8%	15.4%
13	WAG	3 Phase WAG	Stone II	0.78	59.2%	5.9%
14	WAG	3 Phase WAG	Stone I	0.5	67.0%	15.7%
15	WAG	3 Phase WAG	Stone I	1	65.4%	13.0%
16	WAG	3 Phase WAG	Stone I	2	63.1%	9.0%

Table III- Summary of simulation results for the PUNQ-S3 test case.

Case	Recovery Scheme	Hysteresis Model	Interpolation Model	Land Parameter (C)	% Recovery	% Difference from base case
1	**WAG-PUNQS3 (Base Case)**	None	Default	N/A	53.9%	0.0%
2	**WAG-PUNQS3 (Base Case)**	None	Stone I	N/A	57.7%	0.0%
3	**WAG-PUNQS3 (Base Case)**	None	Stone II	N/A	53.0%	0.0%
4	WAG-PUNQS3	Carlson	Stone I	N/A	59.3%	2.8%
5	WAG-PUNQS3	3P WAG model	Stone I	0.78	62.9%	9.0%

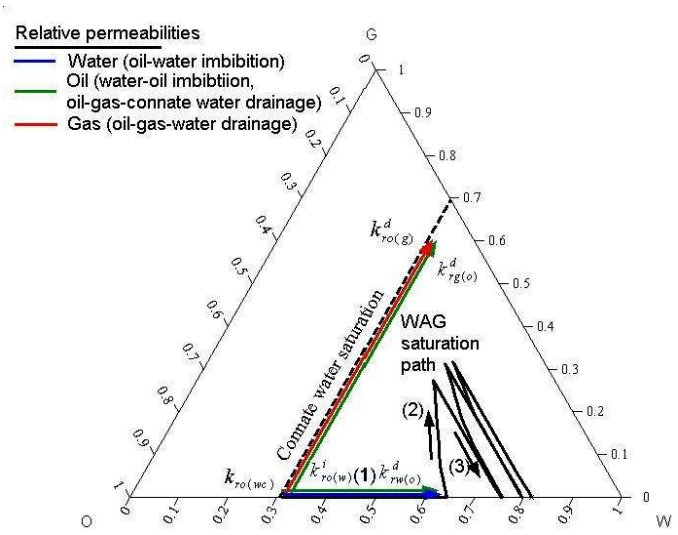

Fig. 1— Typical saturation path in a WAG displacement process, and common two-phase relative permeability input data for simulation.

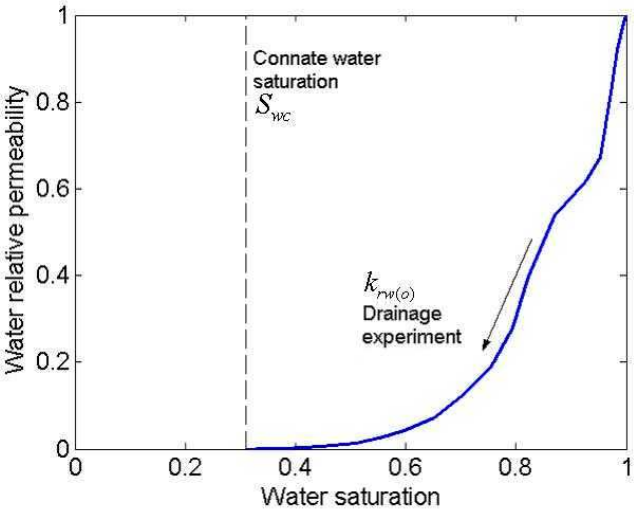

Fig. 2— Water relative permeability from an oil-water drainage experiment.

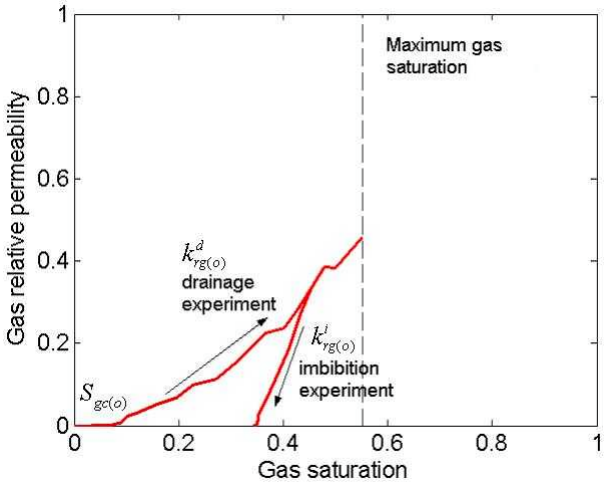

Fig. 3— Gas relative permeability from an oil-gas-connate water experiment.

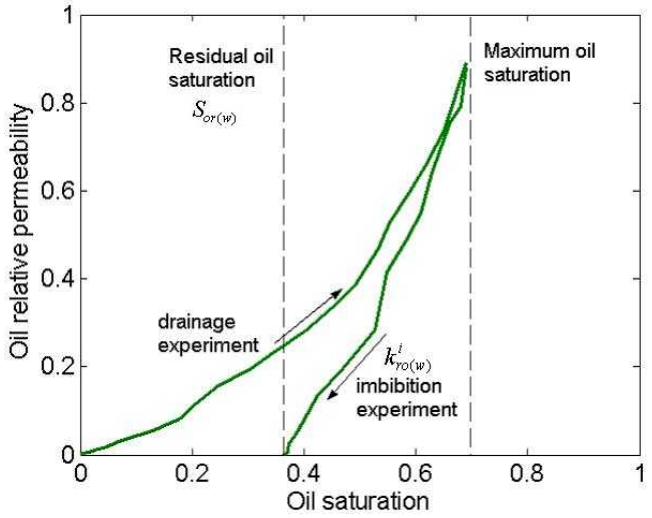

Fig. 4— Oil relative permeabilities from an oil-water drainage and imbibition experiment.

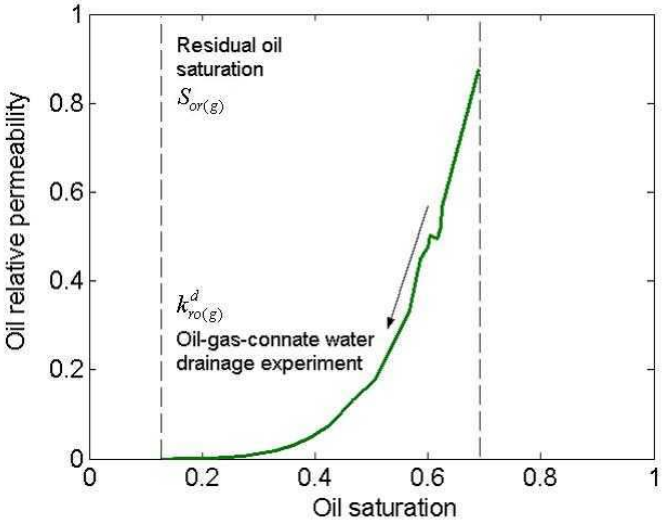

Fig. 5— Oil relative permeabilities from and oil-gas-connate water drainage experiment.

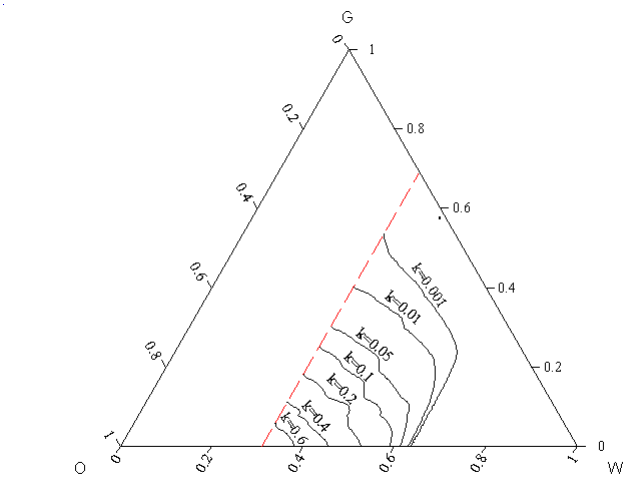

Fig. 6— Oil isoperms predicted by the Stone I model.

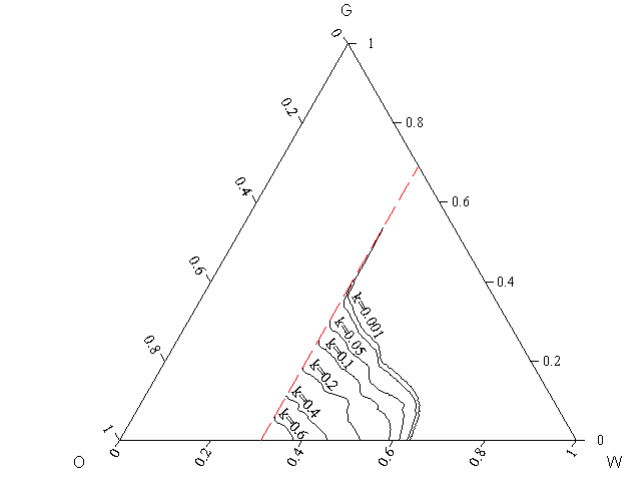

Fig. 7— Oil isoperms predicted by the Stone II model.

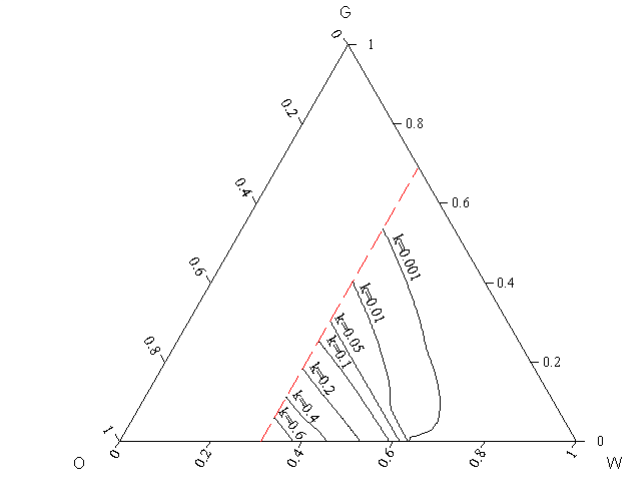

Fig. 8— Oil isoperms predicted by the Baker model.

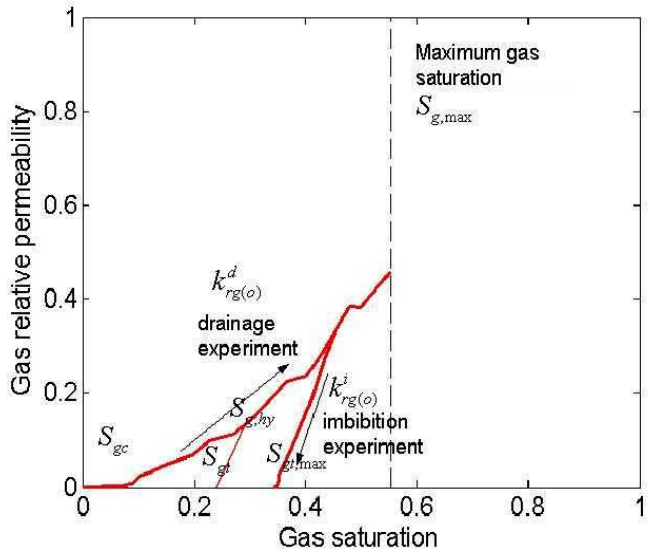

Fig. 9— Critical end point saturations to evaluate Land trapping coefficient.

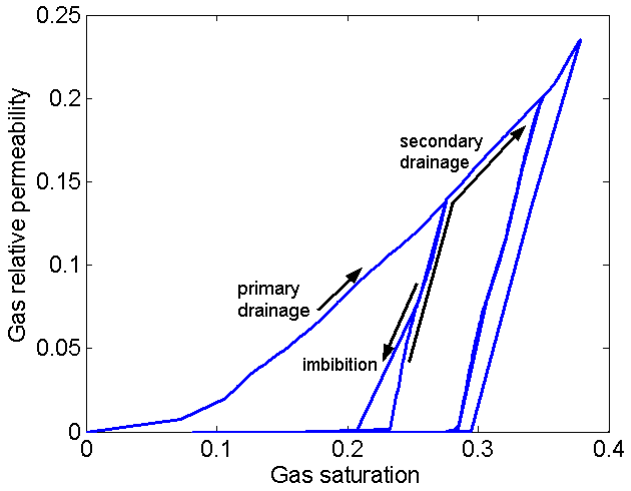

Fig. 10— Relative permeability curves in drainage-imbibition cycles, calculated from the two-phase Carlson hysteresis model.

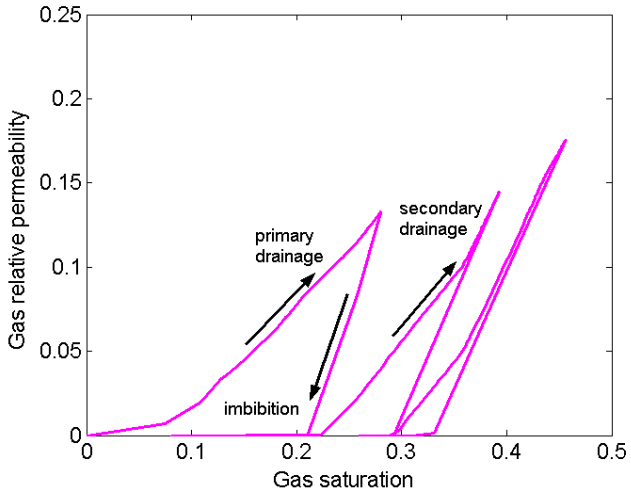

Fig. 11— Gas relative permeability scanning curves calculated with a three-phase hysteresis model.

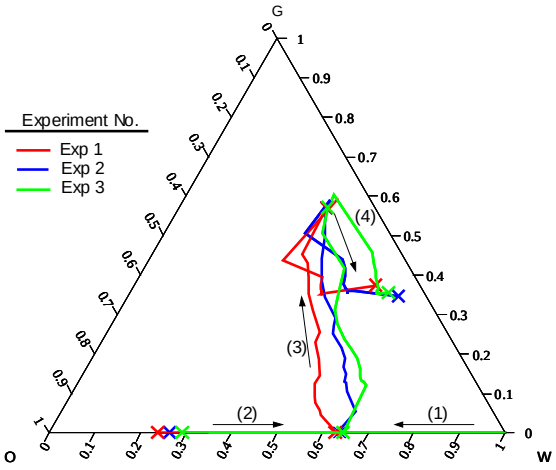

Fig. 12— Saturation paths of selected experiments from Oak's relative permeability data.

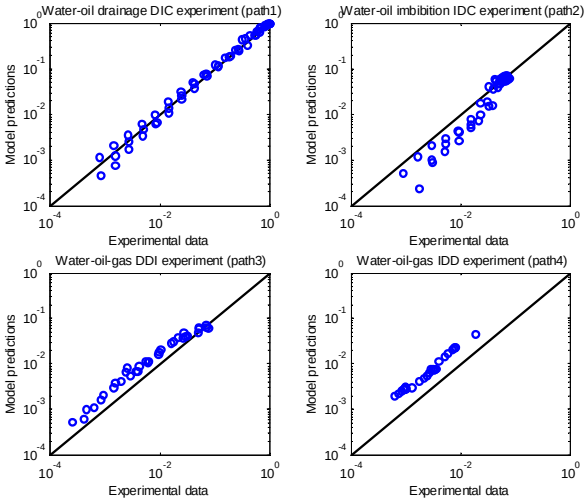

Fig. 13— Correlation between modeled and experimental water relative permeabilities for each displacement path.

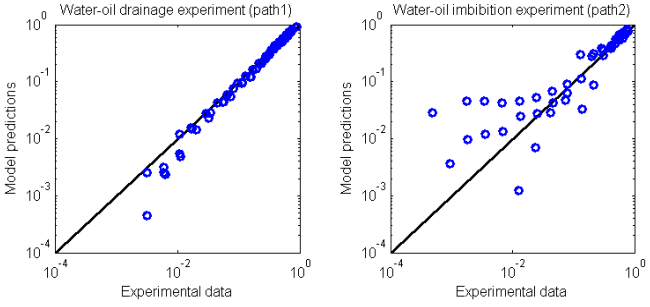

Fig. 14— Correlation between modeled and experimental oil relative permeability for two-phase displacement (paths 1 and 2).

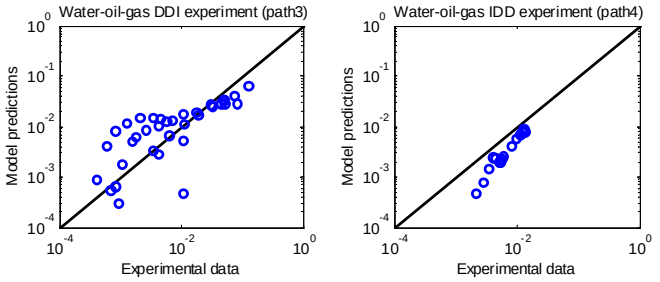

Fig. 15— Correlation between Stone I interpolation and experimental relative permeabilities, with a residual oil model given by Equation 7.

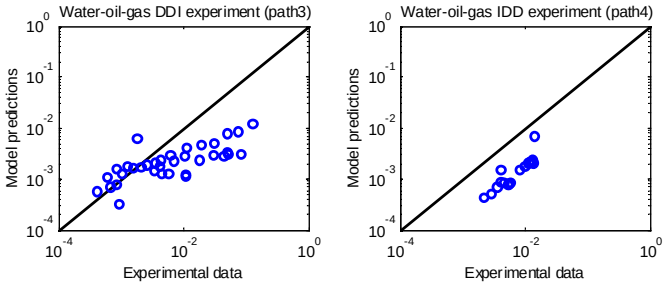

Fig. 16— Correlation between Baker interpolation model and experimental relative permeabilities.

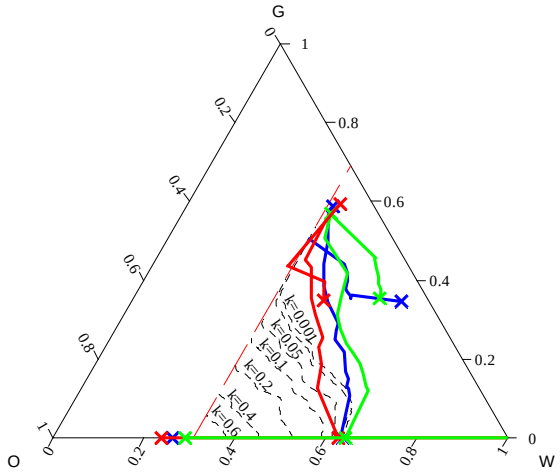

Fig. 17— Oil isoperms predicted by the Stone II model and experimental data paths.

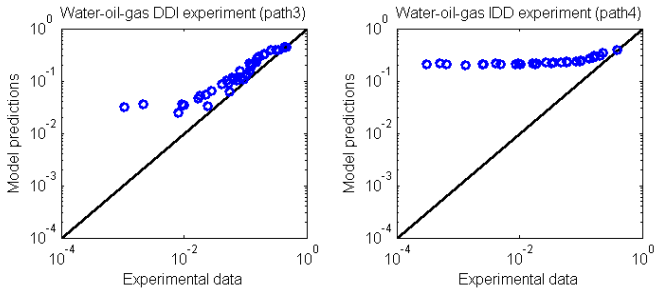

Fig. 18— Comparison of gas relative permeability for different three-phase displacements (paths 3 and 4) with the two-phase gas relative permeability from an oil-gas drainage experiment.

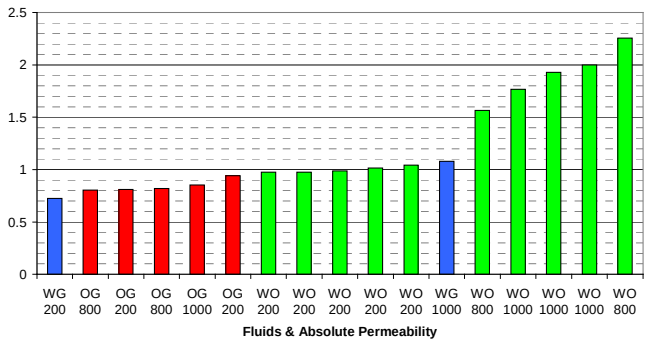

Fig. 19— Land trapping coefficient calculated from two-phase data, with different pairs of fluids (water (W), oil (O), gas (G)) and rock permeability (200, 800, 1000 md).

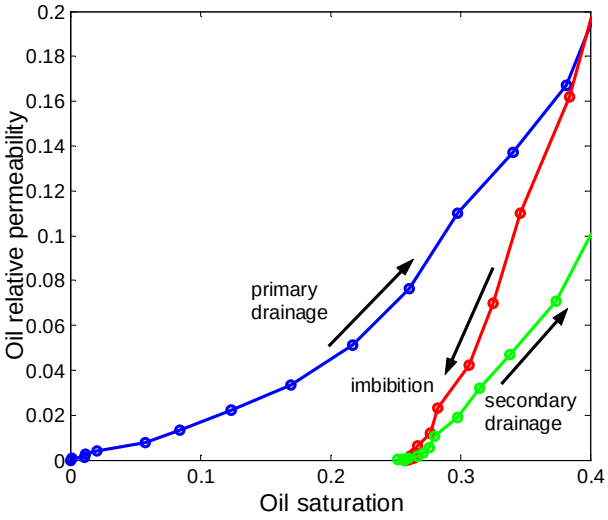

Fig. 20— Oil relative permeability in an oil-water experiment, showing irreversibility of the imbibition scanning curve.

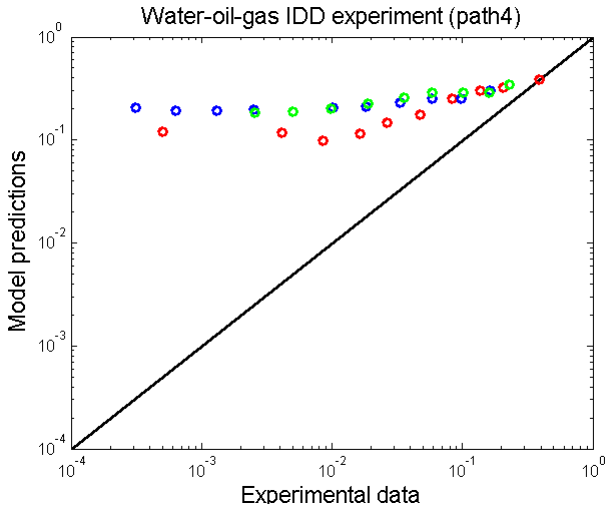

Fig. 21— Scatter plot for Killough's two-phase hysteresis model for a three-phase imbibition process (path 4).

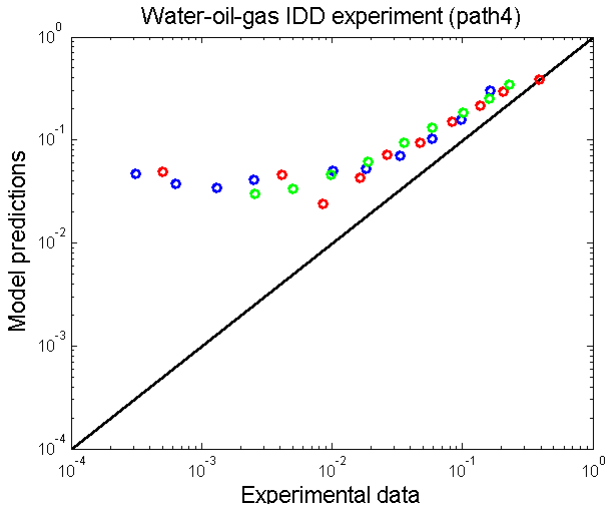

Fig. 22— Scatter plot for Carlson's two-phase hysteresis model for a three-phase imbibition process (path 4).

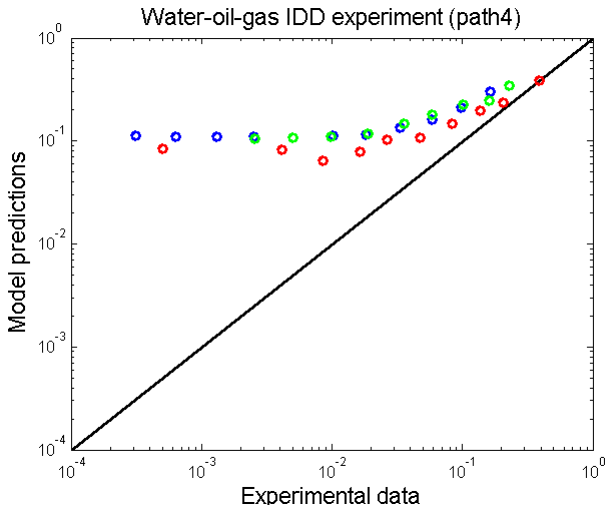

Fig. 23— Scatter plot of gas relative permeability predicted by the WAG three-phase hysteresis model for a three-phase imbibition process (path 4).

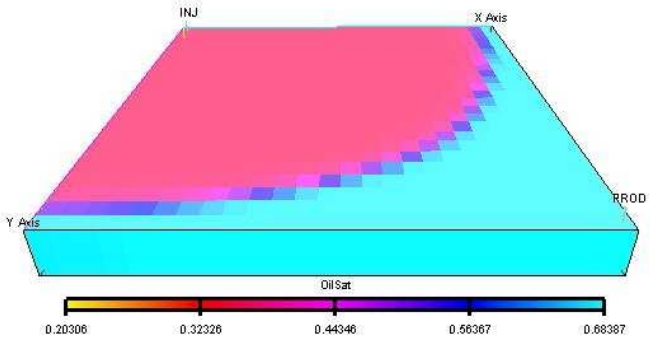

Fig. 24— Three-dimensional view of the synthetic model.

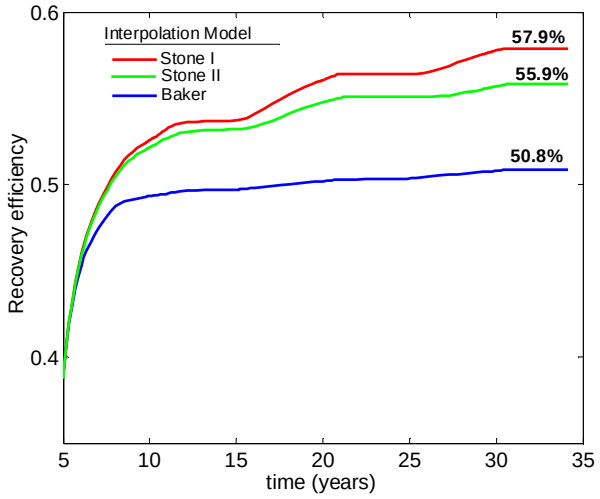

Fig. 25— Recovery efficiency for the synthetic case, using different oil relative permeability interpolation models.

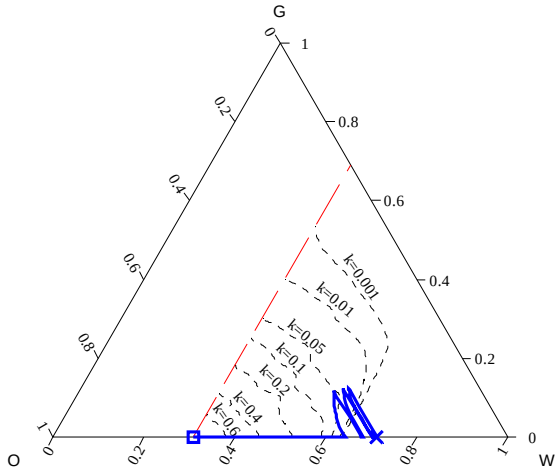

Fig. 26— Oil isoperms calculated by the Stone I model, and saturation path in grid block (12,12,1) of the synthetic reservoir.

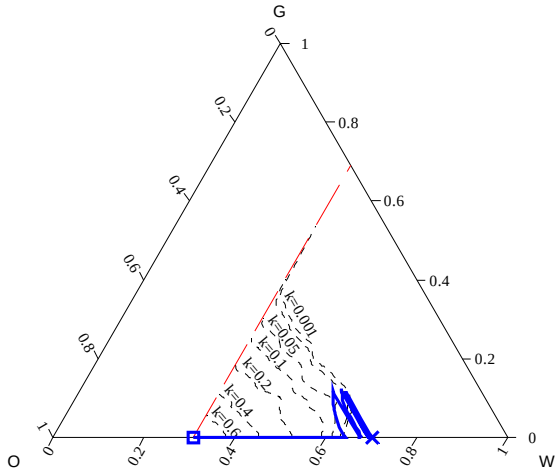

Fig. 27— Oil isoperms calculated by the Stone II model, and saturation path in grid block (12,12,1) of the synthetic reservoir.

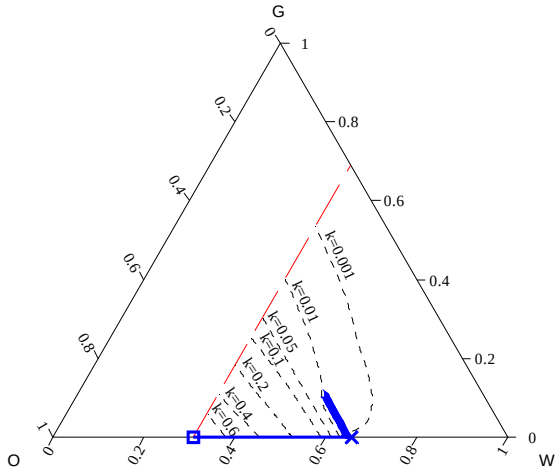

Fig. 28— Oil isoperms calculated by the Baker model, and saturation path in grid block (12,12,1) of the synthetic reservoir.

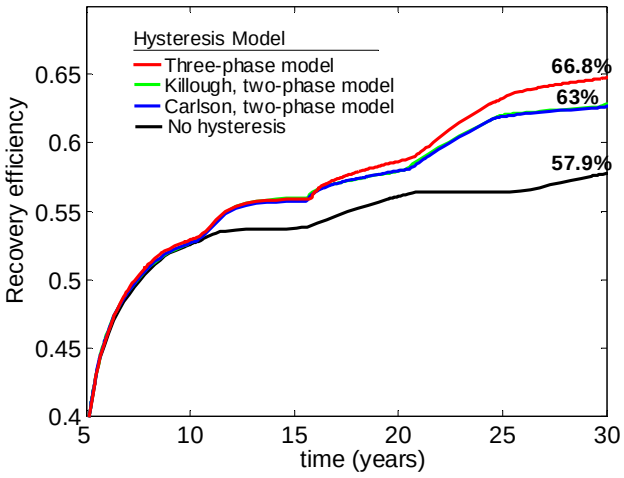

Fig. 29— Recovery efficiency predicted by each hysteresis model using the Stone I interpolation model.

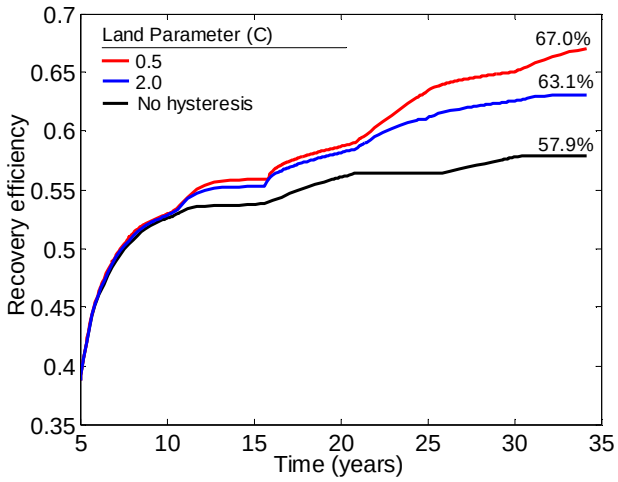

Fig. 30— Recovery efficiency for the WAG three-phase model and the Stone I interpolation model, using different Land trapping coefficients.

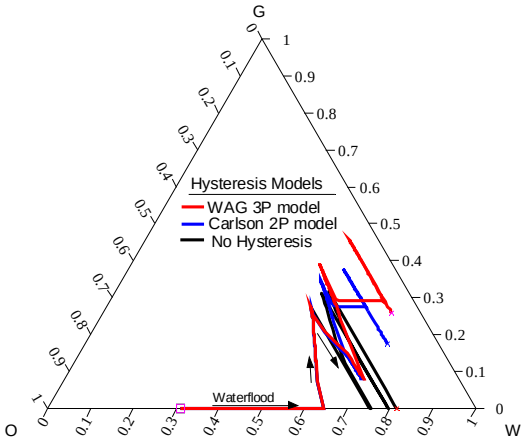

Fig. 31— WAG saturation path at grid block (2,2,1) for different hysteresis models, using Stone I interpolation model.

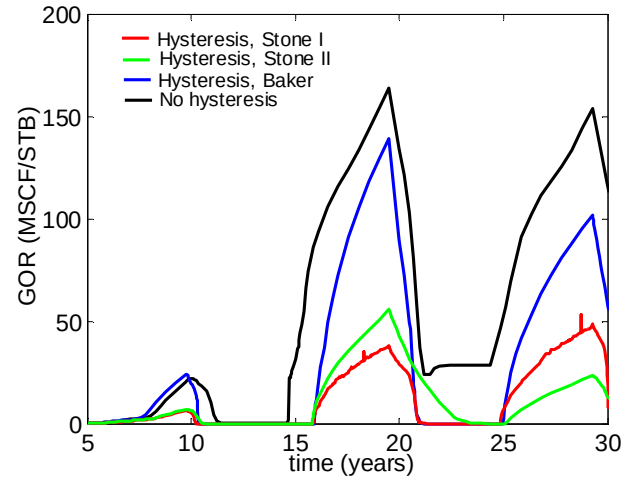

Fig. 32— Gas-oil ratio using the three-phase WAG hysteresis model for different interpolation models.

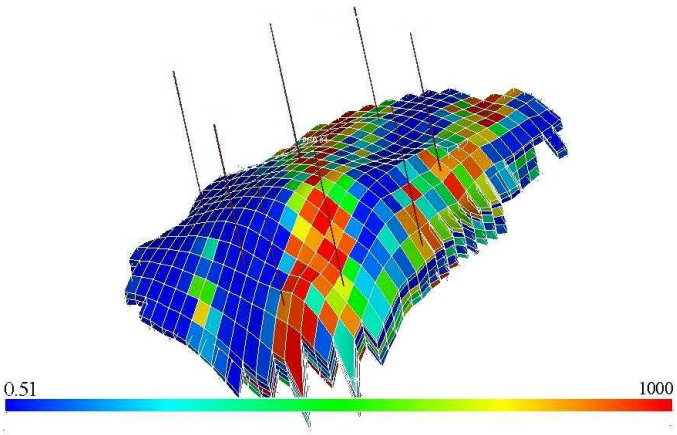

Fig. 33— Horizontal permeability distribution (md) of the PUNQ-S3 model.

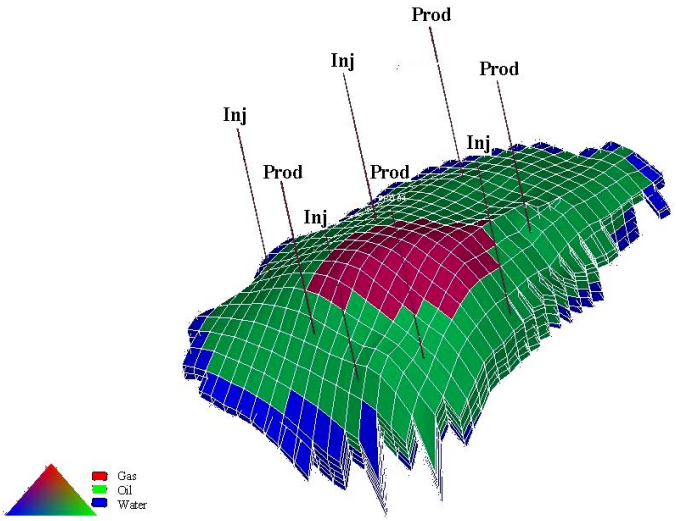

Fig. 34— Initial fluid distribution and location of injection and production wells in the PUNQ-S3 model.

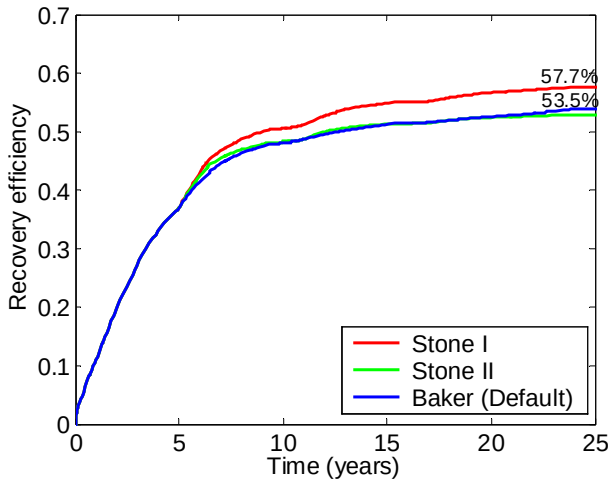

Fig. 35— Recovery efficiency in the PUNQ-S3 reservoir model for different interpolation models, without hysteresis.

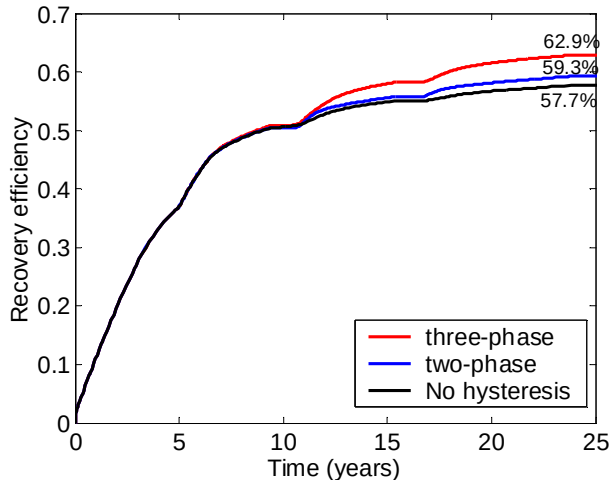

Fig. 36— Recovery efficiency in the PUNQ-S3 reservoir model for different hysteresis models, and the Stone I interpolation model.